



The potential and challenges of the ‘RUSLE-IC-SDR’ approach to identify sediment dynamics in a Mediterranean catchment

Niguse Abebe^{a,c,d,*}, Joris Eekhout^b, Bart Vermeulen^a, Carolina Boix-Fayos^b, Joris de Vente^b, Berhane Grum^c, Ton Hoitink^b, Jantiene Baartman^d

^a Hydrology and Quantitative Water Management Group, Wageningen University, Wageningen, the Netherlands

^b Soil and Water Conservation Research Group, CEBAS-CSIC, Murcia, Spain

^c School of Civil Engineering, Mekelle University, Mekelle, Tigray, Ethiopia

^d Soil Physics and Land Management Group, Wageningen University, Wageningen, the Netherlands

ARTICLE INFO

Keywords:

Soil erosion-RUSLE

Index of sediment connectivity

Sediment delivery ratio

Sediment yield

Hotspot location

ABSTRACT

Soil erosion is a natural process that can be accelerated by natural and anthropogenic disturbances and lead to land degradation and geomorphological changes. Analyzing soil erosion and catchment sediment dynamics is a complex process. In such cases, simplified methods can be applied to analyze soil erosion and sediment connectivity variations and to understand sediment flux in a river basin to inform watershed management. In this study, we tested the combined method of the Revised Universal Soil Loss Equation (RUSLE), the Index of Connectivity (IC), and the Sediment Delivery Ratio (SDR) to estimate sediment yield (SY) and investigate the spatiotemporal variation of soil erosion rates and sediment connectivity in the Mediterranean Rogativa catchment ($\sim 53 \text{ km}^2$), Southeast Spain. In this ‘RUSLE-IC-SDR’ approach, the sediment delivery ratio was estimated from the spatially distributed index of connectivity, calculated using SedInConnect and accounting for the trapping efficiency of 58 check dams in the channels, while assuming 100 % sediment delivery in other parts of the channels. The sediment delivery ratio was calibrated, and sediment yield was verified for the year 2001 using observed sediment yield (in 2003) behind the non-silted check dams. Predicted soil erosion, connectivity (IC, SDR, and SY), and soil erosion-connectivity maps were quantified and compared over time and space, revealing the impacts of rainfall, land use, and check dams. These maps show higher values for areas closer to the channels than on the hillslopes, and higher values on croplands than other land use types, as well as a decrease over time due to land use change and the construction of check dams. The relatively simple ‘RUSLE-IC-SDR’ approach was found to be effective in identifying the sources and hotspots on the hillslopes of a complex Mediterranean catchment. Future studies should consider the channel erosion processes as the RUSLE-IC-SDR does not take these into account.

1. Introduction

Hydrological, geomorphological, and geochemical processes such as discharge, soil erosion, nutrient retention, and sediment transport in watersheds and river channels are essential for retaining environmental and socio-economic services (Costigan et al., 2017; Jaeger et al., 2017; Levick et al., 2008). Soil erosion is a natural process that can be accelerated by natural and anthropogenic disturbances such as changes in climate, land cover, and management practices, which may lead to land degradation and geomorphological change (Ouadja et al., 2022, 2021; Rahmati et al., 2022; Rajbanshi and Bhattacharya, 2020; Rellini et al.,

2019). The spatial distribution of soil erosion rates can be analysed through field monitoring and modelling. As some soil erosion models are quite data-demanding, often simple models such as the Revised Universal Soil Loss Equation (RUSLE) are applied.

The interaction of soil erosion and sediment transport processes with the hydrological and geomorphological processes include sediment generation, detachment, transport, and deposition (Bracken et al., 2015, 2013; Thompson et al., 2013; Turnbull and Wainwright, 2019). These processes illustrate the erosional responses of a landscape and sediment transport at different spatial and temporal scales and highlight the vital role of land use, climate, and topography (Najafi, et al., 2021b; Rainato

* Corresponding author: Wageningen University and Research, Postal address: 6708 PB, Lumen (Building no. 100), Wageningen, the Netherlands.
E-mail address: niguseabebe.hagos@wur.nl (N. Abebe).

et al., 2018).

Over the last decades, sediment connectivity has emerged as a paramount property of geomorphic systems to help understand hydrology and sediment dynamics (Bracken et al., 2015; Fryirs, 2013; Keesstra et al., 2018; Wohl et al., 2019). In line with Heckmann et al. (2018); connectivity can be defined as the degree to which a system facilitates the transfer of sediment and water in a catchment at a given moment. The sediment connectivity signature helps to understand, visualize, and quantify sediment flux in a river basin (Calsamiglia et al., 2018; Crema & Cavalli, 2018; Cucchiaro et al., 2019; Grauso et al., 2018; Hooke, 2003; Keesstra et al., 2018; Parsons et al., 2015; Poepll et al., 2020; Wainwright et al., 2015).

Although sediment connectivity is widely accepted as a descriptor of the link between geomorphic characteristics and sediment transport, there is still no consensus on how to quantify and compare connectivity at different spatial and temporal scales and among distinct landscape properties (Hooke et al., 2021; Hooke & Souza, 2021; Najafi et al., 2021a; Wohl, 2017). Diverse methods and techniques to analyze connectivity have been developed and applied at various study area sizes, using different data resolutions, and calculating various sediment connectivity indices, to understand morphological processes (Hooke et al., 2021; Najafiet al., 2021a).

The Index of Connectivity (IC) is a dimensionless indicator that assesses the potential of sediment arrives at user-defined targets (e.g., roads, streams) and sinks (e.g., outlet, ponds, lakes, check dams, reservoirs) (Crema and Cavalli, 2018; Persichillo et al., 2018). However, the IC does not quantify erosion and sediment transport itself (e.g., in t/ha), as erosion models do (Batista et al., 2019; de Vente et al., 2013; Hajigholizadeh et al., 2018; Merritt et al., 2003; Pandey et al., 2016). Many hillslope erosion models, such as the RUSLE, however, focus on hillslope processes, disregarding sediment transport from hillslopes to channels. Therefore, there is potential interest to combine hillslope soil erosion models with the relatively simple IC (Hamel et al., 2015) to assess sediment delivery through a catchment. Crema & Cavalli (2018) developed a modified standalone tool called SedInConnect by introducing different weighting factors and rearranging the original IC as proposed by Borselli et al. (2008). SedInConnect has relatively low data requirements and can be applied at the catchment scale to quantify the intensity and degree of structural sediment connectivity, and has been used extensively (Hooke et al., 2021).

Vigilak et al. (2012) introduced a method to estimate the Sediment Delivery Ratio (SDR) from the IC, to explain hillslope sediment transport potential. The SDR is defined as the ratio between sediment yield at a watershed outlet and the average annual soil loss across its upstream area (Maner, 1958; Walling, 1983; Wu et al., 2018). The spatially distributed SDR can subsequently be used to determine the sediment yield (SY) when coupled with the RUSLE model (Hamel et al., 2017, Hamel et al., 2015). Various studies applied the RUSLE-IC-SDR approach with this purpose (Hamel et al., 2017; Michalek et al., 2021; Rajbanshi & Bhattacharya, 2020; Woznicki et al., 2020; Zhao et al., 2020). Zhao et al. (2020) applied the RUSLE-IC-SDR approach to assess the impact of land use change and check dams on SY in the Yanhe River catchment (7,725 km²) of the Loess Plateau, China and found acceptable model performance on SY estimation. Michalek et al. (2021) also applied this method and analyzed erosion-connectivity patterns in urbanizing settings of Johnson County (1235 km²), Kansas, USA. They concluded that RUSLE model results, with large uncertainties of the C-factor, and IC and SDR were efficient at conveying sediment transfer from source to sink. Moreover, Hao et al. (2022) and Michalek et al. (2021) found that coupling of soil erosion (RUSLE) and IC helps to identify spatial patterns of sediment sources for critical and minimal impact areas that are affected by erosion and deposition. However, most studies had limited opportunity to verify the calculated sediment yield with observed sediment yield. In addition, this combined RUSLE-IC-SDR method was not applied and tested in a Mediterranean catchment to estimate the spatiotemporal variation of sediment yield. In this study, we applied the

RUSLE-IC-SDR method to the Mediterranean Rogativa catchment (~53 km²) in SE Spain. Previous studies in this catchment focused on geomorphic channel forms, organic carbon stock dynamics, land use changes and check dams impacts (Halifa-Marín et al., 2019; Nadeu et al., 2014, 2015; Boix-Fayos et al., 2007; Boix-Fayos et al., 2008). Besides, the Rogativa catchment was included in wider-scale studies by Quiñonero-Rubio et al. (2016), Boix-Fayos et al. (2020), and Ekhout et al. (2020) on the impact of land use and climate changes on soil erosion, sediment yield, carbon dynamics, and related ecosystem services.

We used the previous insights to quantify and compare soil erosion rates, sediment connectivity, and sediment yield in the Rogativa catchment and evaluate the added value of the RUSLE-IC-SDR methodology. The Mediterranean Rogativa catchment (SE Spain) is characterized by complex geomorphology with significant changes in hillslope and channel morphological processes induced by important land use changes over the past 60 years (Boix-Fayos et al., 2007). The Rogativa catchment is particularly useful to test the ‘RUSLE-IC-SDR’ approach because of the available sediment yield data, obtained in 58 check dams (Boix-Fayos et al., 2007) that allows to critically evaluate the method. There are limited studies globally and no studies in the Mediterranean catchments applying the simple and combined ‘RUSLE-IC-SDR’ approach to estimate the spatiotemporal variation of sediment yield in geomorphological complex catchments.

The objectives of this study were: (i) to test the ‘RUSLE – IC – SDR’ approach in the Mediterranean Rogativa catchment using observed sediment yield data and (ii) to investigate spatial and temporal changes (1952–2018) of soil erosion rate and sediment connectivity, and the role of land use change, rainfall variations, and check dam construction in the catchment.

2. Material and methods

2.1. Description of the study area

The study catchment, Rogativa, is located in SE Spain at 38° 08'N, 2° 13'W. It is a sub-catchment of the Taibilla, a tributary of the Segura River, located in the Betic Mountains in Murcia province, Southeast Spain (Fig. 1). The catchment covers an area of ~53 km² with elevations ranging between 1025 m and 2013 m a.s.l., an average slope of 29°, and longest flow path of 17.77 km. The Rogativa catchment has a dry to subhumid Mediterranean climate with a mean annual temperature of 13.3 °C, and minimum, mean, and maximum annual rainfall of 445, 577, and 735 mm for the period 1952–2018, respectively (Ekhout et al., 2020). Lithology consists of marls in the valley floors and limestones on higher elevations (IGME, 1978). Soils in the catchment are mostly classified as Regosols. Some Leptosols are found at higher elevations and Cambisols on the north-facing slopes under forest cover (Alías, 1991).

Although the main stream of the Rogativa catchment is often intermittent, it can have continuous flow for several months during humid years (Boix-Fayos et al., 2007). Land use and land cover (LULC) changes occurred in the Rogativa catchment due to the abandonment of agricultural areas, afforestation, and construction of check dams (Boix-Fayos et al., 2007).

Fig. 2 and Table 1 show the land use and land cover changes between 1956 and 2016 based on previous studies (Boix-Fayos et al., 2007; Ekhout et al., 2020). In the Rogativa catchment, 58 check dams were constructed between 1976 and 1978 (Fig. 1c). Fig. 1d shows a picture of a typical check dam. A detailed description of the study area can be found in Boix-Fayos et al. (2008) and Boix-Fayos et al. (2007).

2.2. Soil erosion and sediment connectivity calculations

The overall methodological framework to quantify soil erosion and sediment connectivity and the link between soil erosion and sediment connectivity for the Rogativa catchment is presented in Fig. 3. Soil erosion and sediment connectivity were analyzed for the four time

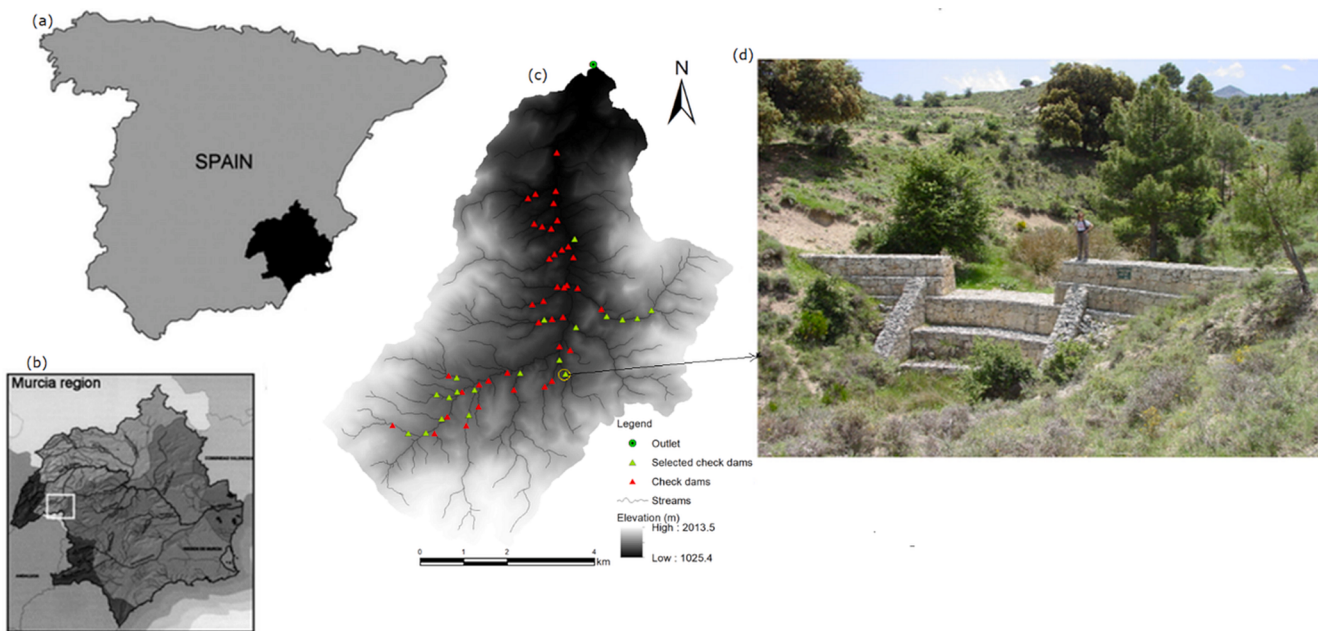


Fig. 1. Location of the Rogativa catchment (c) in Murcia region (b), SE Spain (a). An example of a check dam in the Javanas ravine in the upstream area of the catchment (d) (a and b modified after Boix-Fayos et al. (2007)).

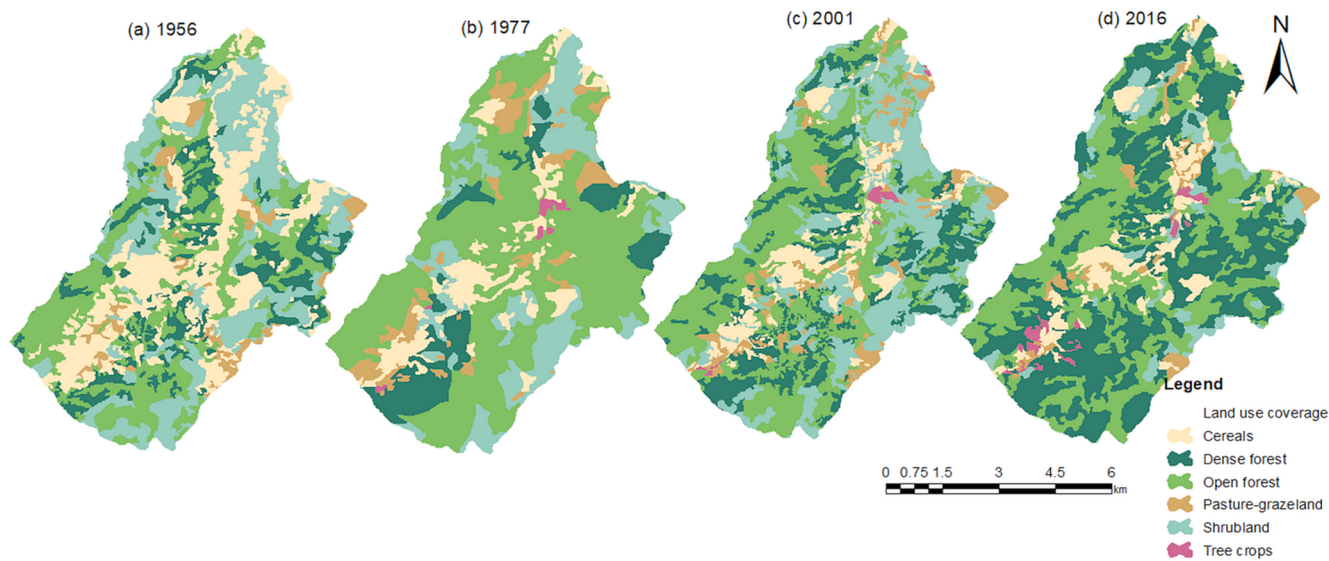


Fig. 2. Land use in the Rogativa catchment in 1956, 1977, 2001, and 2016 (based on Boix-Fayos et al., 2007; Eekhout et al., 2020).

Table 1
Land use, organic carbon content, and C-factor values of different land uses for the four time periods in the Rogativa catchment.

Land use	C-factor	Organic carbon content (%)	Land use coverage (%)			
			1956	1977	2001	2016
Cereals	0.4	4.85	25.4	10.6	10.0	9.9
Dense forest	0.002	6.71	15.3	11.8	20.7	42.2
Open forest	0.004	6.06	28.7	51.7	35.5	35.4
Pasture-grazeland	0.1	5.48	4.8	7.8	7.3	3.8
Shrubland	0.03	5.59	25.7	17.4	25.8	7.4
Tree crops	0.3	5.00	—	0.7	0.6	1.4

periods for which land use maps were available (1956, 1977, 2001, and 2016; Fig. 2). The land use maps of 1977 and 2001 are at a scale of 1:50000 and the 1956 and 2016 maps are at a scale of 1:5000, detailed in Eekhout et al. (2020).

In this study, the following steps were taken (Fig. 3): (1) estimation of soil erosion with the RUSLE (detailed in section 2.2.1); (2) calculation of the IC using the SedInConnect tool for structural connectivity analysis (section 2.2.2); (3) calculation of the SDR from the IC for the hillslopes and retention behind check dams (except 1956) in the channels, assuming 100 % SDR in the channels themselves (section 2.2.4); (4) combining (1) and (2) to assess soil erosion-connectivity patterns (section 2.2.3); (5) combining (1) and (3) to estimate sediment yield using a sediment accumulation algorithm (section 2.2.4).

2.2.1. Annual soil loss estimation using RUSLE

The spatial distribution of soil erosion (sheet and rill erosion) rates in

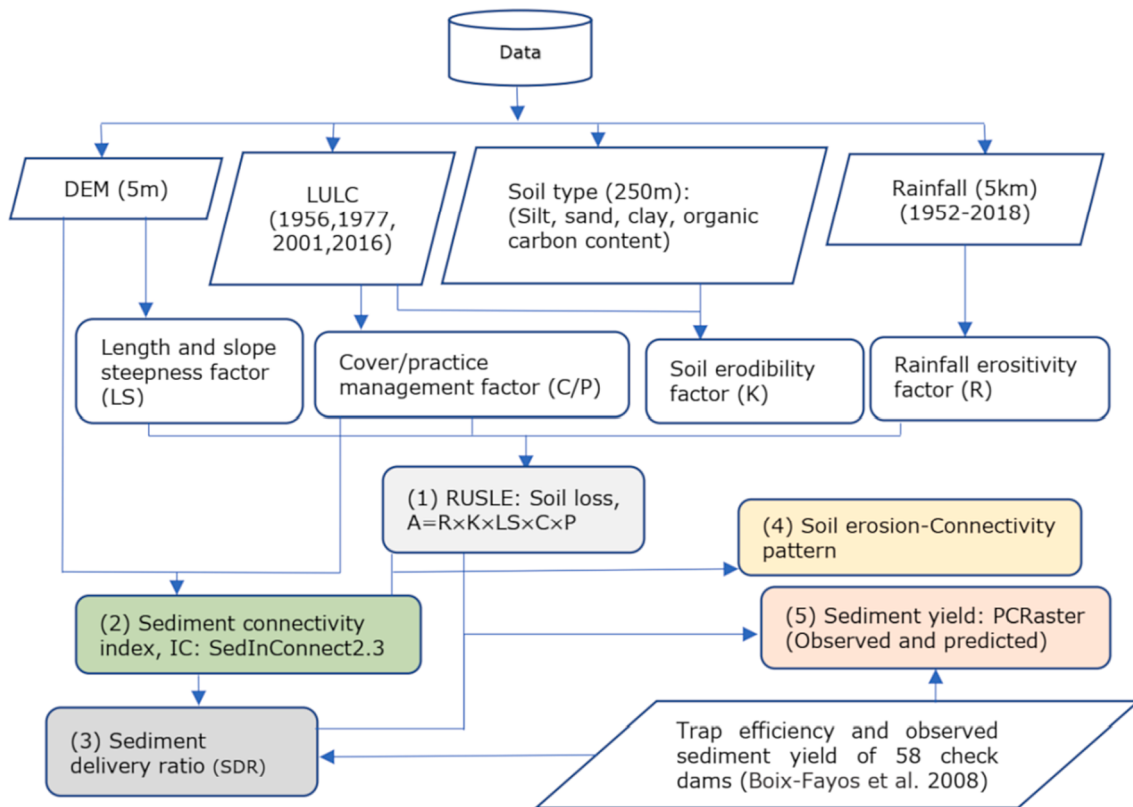


Fig. 3. The methodological framework for the analysis of soil erosion and connectivity in the Rogativa catchment, SE Spain. Trapezoidal boxes refer to input data; white boxes are intermediate products derived from the input data and required for the calculation of hillslope erosion (1), IC (2), and SDR (3). Hillslope erosion and IC are combined to obtain the erosion-connectivity pattern (4), and soil erosion and SDR are combined to derive sediment yield (5).

the Rogativa catchment was analysed using the RUSLE model (eq. (1)).

$$A = R \times K \times LS \times C \times P \quad (1)$$

where A is annual soil loss ($\text{t ha}^{-1} \text{yr}^{-1}$), R is the rainfall erosivity factor ($\text{MJ mm ha}^{-1} \text{h}^{-1} \text{yr}^{-1}$), K is the soil erodibility factor ($\text{t h MJ}^{-1} \text{mm}^{-1}$), L (-) and S (-) are the slope length and slope gradient factors, respectively, C (-) is the cover management and P (-) is the soil conservation practice factors of a grid cell.

Each of the six RUSLE factors was computed as a spatially distributed variable. The rainfall erosivity factor (R) was determined using eqs. (2) and (3) following Renard & Freimund (1994).

$$R = \begin{cases} 0.7397MFI^{1.847}, & \text{if } MFI < 55\text{mm} \\ 95.77 - 6.081MFI + 0.4770MFI^2, & \text{if } MFI > 55\text{mm} \end{cases} \quad (2)$$

where MFI (Modified Fournier Index) in mm, defined by Arnaldus (1977).

$$MFI = \frac{\sum_{i=1}^{12} P_i^2}{P} \quad (3)$$

where P_i is the average monthly precipitation (mm), and P is the average annual precipitation (mm) at a grid cell.

In the present study, we used precipitation data for the period 1952–2018 with a 5 km resolution obtained from Peral García et al. (2017). The rainfall map was resampled using the bilinear technique to obtain a similar resolution as the DEM (Digital Elevation Model; 5 m). The R factor was then calculated for 4 time periods (1952–1967, 1968–1984, 1985–2001, and 2002–2018) corresponding with the four land use maps (1956, 1977, 2001, and 2016; Fig. 2).

The soil erodibility factor (K) characterizes the resistance of soil to erosion. The K factor was estimated using eq. (4) based on soil texture and soil organic carbon data (Sharpley and Williams, 1990):

$$K = 0.1317 \times \left[0.2 + 0.3e^{-0.256m_s \left(1 - \frac{m_{silt}}{100} \right)} \right] \times \left[\frac{m_{silt}}{m_c + m_{silt}} \right]^{0.3} \times \left[1 - \frac{0.25 * orgC}{orgC + e^{3.72 - 2.95orgC}} \right] \times \left[1 - \frac{0.7 \left(1 - \frac{m_s}{100} \right)}{\left(\frac{1 - m_s}{100} \right) + e^{-5.51 + 2.95 \left(1 - \frac{m_s}{100} \right)}} \right] \quad (4)$$

where K is the soil erodibility index ($\text{t h MJ}^{-1} \text{mm}^{-1}$), m_s , m_{silt} and m_c are % sand (0.05–2 mm), silt (0.002–0.05 mm), and clay (<0.002 mm), respectively, and $orgC$ is the % organic carbon content. Soil texture and organic matter content data with a 250 m resolution were obtained from the SoilGrids database (Hengl et al., 2017). The mean value of organic carbon content was assigned for the four land use types of 1956, 1977, 2001, and 2016. Table 1 lists the $orgC$ values per land use type.

The topographic factors are usually combined as LS (Length and steepness). Both factors were calculated using a LiDAR-derived DEM with a 5 m resolution obtained from Ministerio de Fomento de España (2015). In this study, the LS-tool multiple-flow direction (MFD) algorithm developed by Zhang et al. (2017) was applied with an area of 0.5 ha as a threshold for the contributing area.

The vegetation cover factor (C-factor; Table 1) for each land use type was adopted from de Vente et al. (2009) and Nadeu et al. (2014). There are no significant conservation practices throughout the study catchment, except for check dams which are not accounted for in the RUSLE, therefore, the erosion control practice factor (P-factor) was set to 1 (Eekhout and de Vente, 2020; Panagos et al., 2015).

2.2.2. Index of connectivity calculation

IC was computed using SedInConnect 2.3, a stand-alone, and open-source software developed by Crema & Cavalli (2018) based on the original work of Borselli et al. (2008), after hydrologically conditioned

(pit removed) using the TauDEM tool (Tarboton et al., 2015).

The topography-based IC proposed by Borselli et al. (2008) incorporates the characteristics of the contributing area (upstream component – D_{up}), and the local potential for downward routing of the sediment, and the characteristics of the flow path to be performed by the sediment to the point of interest (downstream component - D_{dn}), which is used to depict the spatial distribution of potential sediment transport pathways. The IC values of each cell are presented in an interval of $[-\infty, + \infty]$, with connectivity increasing for larger IC values as calculated using eq. (5).

$$IC = \log_{10} \frac{D_{up}}{D_{dn}} = \log_{10} \left(\frac{\bar{W}\bar{S}\sqrt{A}}{\sum_i \frac{d_i}{W_i S_i}} \right) \quad (5)$$

where D_{up} is the upslope component, D_{dn} is the downslope component, W_i is the weighting factor for the i^{th} cell (dimensionless), \bar{W} is the average weighting factor of the upslope contributing area (dimensionless), A is the upslope contributing area (m^2), d_i is the length of the i^{th} cell along the steepest downslope path to the sink (m), S_i is the slope gradient of the i^{th} cell, and \bar{S} is the average slope gradient of the upslope contributing area (m/m).

In this study, the RUSLE C-factor (Table 1) was used as the weighting factor, as a proxy for impedance to sediment fluxes in the IC computation. Streams with a maximum threshold contributing area of 5 ha were used as the target for the IC calculation (Michalek et al., 2021; Mishra et al., 2019).

2.2.3. Linking erosion and connectivity

Erosion-Connectivity (E-C) interaction was assessed by combining maps of RUSLE-derived soil erosion estimates (E) and connectivity (here, C refers to IC) patterns to identify critical and contrasting areas and show hotspot areas in sediment sources (Hao et al., 2022; Michalek et al., 2021). Based on Hao et al. (2022) and Michalek et al. (2021), we identified four quadrants of severity level to analyse the soil erosion-connectivity (E-C) linkage: high erosion-high connectivity (HE-HC), high erosion-low connectivity (HE-LC), low erosion-high connectivity (LE-HC), low erosion-low connectivity (LE-LC). High erosion-high connectivity (HE-HC) is a critical region that potentially needs interventions to mitigate soil erosion and sediment transport.

Low, medium, and high soil erosion rate classes (Jenks, 1967) were set as <1, between 1 and 10, and greater than $10 \text{ t ha}^{-1} \text{ yr}^{-1}$, respectively. The IC values were classified using the 10th percentile (P_{10}) as low connectivity, P_{10} – P_{90} as medium connected, and greater than 90th percentile (P_{90}) as highly connected. Classified maps of RUSLE erosion rates and IC were then combined into the four quadrants mentioned above.

2.2.4. Sediment delivery ratio and sediment yield calculation

The SDR and SY have been used as indicators of functional sediment connectivity (Najafi et al., 2021a; Zhao et al., 2020). Here, SDR was derived from IC using a sigmoid function (Hamel et al., 2015, 2017; Vigiak et al., 2012; Zhao et al., 2020) as described in eq. (6).

$$SDR = \frac{SDR_{Max}}{1 + exp\left(\frac{IC_0 - IC}{k_b}\right)} \quad (6)$$

where SDR_{Max} is the maximum theoretical SDR with a range of 0 to 1.0, defined as the maximum proportion of fine sediment (<1000 μm) traveling to the stream; SDR_{Max} was assumed 1 for this study at cell scale (Vigiak et al., 2012). IC_0 and k_b are landscape-independent and landscape-dependent calibration parameters, respectively, that define the shape of the sigmoid function of the SDR-IC relationship (Hamel et al., 2015; Vigiak et al., 2012). As the channels were set as targets for IC calculation, no SDR is calculated for the streams. We assumed the

streams to be fully connected, corresponding to an SDR of 1 (Hao et al., 2022), except for locations in the stream network where check dams are located, which reduce the channel connectivity.

In 1976–1977, 58 check dams were constructed in the catchment. Their effect on sediment yield and thus sediment connectivity, was considered (except for the year 1956) by calculating the trapping efficiencies (TEs) of the check dams. TE for a single check dam can be estimated using the empirical sediment retention function developed by Brown (1943) as shown in eq. (7).

$$TE = 100 \left(1 - \frac{1}{1 + 0.0021 D \frac{V}{W}} \right) \quad (7)$$

where V denotes the remaining storage capacity (m^3) of a check dam, W is the contributing catchment area (km^2), and D is a value ranging from 0.046 to 1 (values of $D = 0.046, 0.1$, and 1.0 can be used for fine, medium, and coarse sediments, respectively) suggested by Verstraeten et al. (2007) and Yang & Lu (2018). A value of 0.76 for D was selected for the Rogativa catchment (Boix-Fayos et al., 2008). The sediment portion passing through the check dams was estimated as 1-TE. This passing portion (1-TE) was used as SDR for the channel cells where the check dams were located for the years 1977, 2001, and 2016.

SY estimates based on the accumulated hillslope erosion (RUSLE) with the IC-derived SDR were combined with the assumed full potential delivery (SDR = 1) in the channels, except for locations in the channel where check dams were located. In these locations, the sediment passing factor (1-TE) was used as SDR. Finally, the mean annual sediment yield (SY; t yr^{-1}) was calculated using a sediment routing algorithm using PCRaster (Karssenberg et al., 2010; Zhao et al., 2020). The routing algorithm routes the sediment through the consecutive neighboring downstream cells, following the local drain direction (eq. (8)), and accounts for the fraction of the sediment that is retained in each cell through the SDR.

$$SY = \sum_{i=1}^N A_i \times SDR_i \quad (8)$$

where SY is sediment yield (t yr^{-1}), $\sum_{i=1}^N A_i$ is the total erosion from each source in the watershed (t yr^{-1}), N is the total number of cells in the catchment, and SDR_i denotes the sediment delivery ratio in a specific cell.

2.2.5. Sediment delivery ratio calibration with observed sediment yield data

In the Rogativa catchment, Boix-Fayos et al. (2007) and Boix-Fayos et al. (2008) measured sediment volumes retained behind the 58 check dams and determined the check dams TEs based on their dimensions and contributing area following eq. (7) (Brown, 1943). The measured sediment volumes retained behind check dams together with the TEs of each check dam were used to estimate (specific) sediment yield for each check dam in 2003 (Boix-Fayos et al., 2008).

In the present study, the parameters IC_0 and k_b (Eq. (6)) were calibrated using the observed SY in 2003 of the most upstream 19 non-silted check dams with a relatively high trapping efficiency that were not affected by sediment retention in upstream catchments. In line with the values set originally by Hamel et al. (2015) and Vigiak et al. (2012), values of IC_0 and k_b between 0.0 and 0.5 and 1.0–6.0, respectively, were tested. The prediction of the model was evaluated by comparing observed and simulated SYs and evaluated using Pearson's correlation coefficient (r), correlation coefficient (R^2), Nash-Sutcliffe efficiency coefficient (NSE), Percent bias (PBIAS), and Spearman's rank correlation coefficient (r_s & p). The calibrated IC_0 and k_b values were then applied to predict (S) SY at the subcatchments of the 58 check dams and for the four years (1956, 1977, 2001, and 2016).

3. Results

3.1. Sediment yield verification and 'RUSLE-IC-SDR' linkage

The 'RUSLE-IC-SDR' approach (Hamel et al., 2017) was calibrated by comparing observed (Boix-Fayos et al., 2008) and simulated SY retained behind the selected non-silted check dams for the year 2001 (Fig. 4 and Fig. 5). The best model performance was found for parameter combination $IC_0 = 0.1$ and $k_b = 4.8$ ($R^2 = 0.79$; NSE = 0.51, PBIAS = 0.41, and $r_s = 0.64$ & $p = 0.003$). When using all 58 check dams for calibration, the model showed poorer results (Fig. 4) ($R^2 = 0.55$, NSE = 0.005, PBIAS = 0.78, and $r_s = 0.30$ & $p = 0.024$). The calibration procedure showed that model outputs are more sensitive to calibration parameter k_b than to IC_0 . As k_b expands to a large value the model performance improved. As shown in Fig. 4, there are discrepancies between the SY estimated by the RUSLE-IC-SDR approach and the observed SY. Especially for larger observed SY, the RUSLE-IC-SDR approach underestimates the SY (Fig. 4b).

Fig. 5 shows the observed (Fig. 5a) and simulated (Fig. 5b) SSY per watershed upstream of the 58 check dams. When comparing the observed and simulated patterns (Fig. 5), it appears that the simulations slightly underestimated the SSY in the northwest and eastern hillslopes, while higher SSY was simulated in the center of the catchment. In 2001, the spatial distribution of the soil erosion and sediment connectivity were expressed by RUSLE, IC, SDR, and SSY (Fig. 6). Each of the maps in Fig. 6, shows a consistent spatial pattern, and higher values near the main channel, and in the northeastern part of the Rogatava catchment.

As expected, the hillslope SDR map (Fig. 6c) shows a high similarity to the spatial pattern of the IC map (Fig. 6b). Higher IC and SDR values were estimated for cereal and, to a lesser extent, pasture areas. This reflection of the land cover is directly associated with the C-factor being used as impedance of flow in IC calculations. It is worth noting that cereals and pasture lands have a relatively high C-factor values (Table 1), leading to higher connectivity values compared to forest land cover, for example.

Moreover, the spatial pattern of SY shows much larger sediment values in the channels making the variations in the SY map to be invisible in the hillslopes. In this regard, the results were presented as specific sediment yield (SSY) for each subcatchment representing the SY

per area of upstream contribution for each check dam and the outlet (Fig. 6d).

3.2. Spatiotemporal variation of soil erosion and sediment connectivity

After evaluating the RUSLE-IC-SDR method for 2001 and comparing it with observed SYs behind check dams, here we compare the results of soil erosion and connectivity for the years 1956, 1977, 2001, and 2016. The soil erosion (Fig. 7), and sediment connectivity in terms of IC (Fig. 8), SDR (Fig. 9), and SSY (Fig. 10) show significant spatiotemporal variation in the Rogatava catchment.

The soil erosion rates as estimated using the RUSLE (Fig. 7) were estimated at 20.3, 10.2, 8.3, and 6.7 $t \text{ ha}^{-1} \text{ yr}^{-1}$ for 1956, 1977, 2001, and 2016, respectively (Fig. 7). Thus, soil erosion rates show a drastic decrease from 1956 to 1977 and a slight decrease from 1977 to 2001, and from 2001 to 2016. A higher erosion rate can be seen near the channels, and in cereal cropland areas compared to other land use types.

Fig. 8 shows that IC varied only slightly for the four years (1956, 1977, 2001, and 2016). The mean IC values are -5.14, -5.75, -5.70, and -6.22 in 1956, 1977, 2001, and 2016, respectively. The spatial pattern of the IC maps shows higher values in the croplands compared to other land uses, and higher IC adjacent to the channels as compared to the hillslopes (Fig. 8). Since the channels were considered as a target for IC, the proximity to the streams will inherently give these areas higher IC values as distance to the target is one of the factors in the IC calculation.

The SDR maps (Fig. 9) show a similar spatial and temporal pattern as the IC maps as far as the hillslopes are concerned, as they were computed from IC values (eq. (6)). The combined SDR values of the catchment ranged between 0.01 on parts of the hillslopes to 1 in the streams, and maximum value of 0.56 on the hillslopes. The spatial average of the combined SDRs for the Rogatava catchment was 0.266, 0.243, 0.244, and 0.227 in 1956, 1977, 2001, and 2016, respectively, indicating a slight overall decrease in SDR over time. The land use (C-factor) and check dams had a significant impact on decreasing the SDR from 1956 to the recent decades. Like the IC pattern, higher SDR values were observed adjacent to streams compared to the hillslopes, which is also to be expected since IC depends on the C-factor; a higher C-factor for cropland results in a higher SDR.

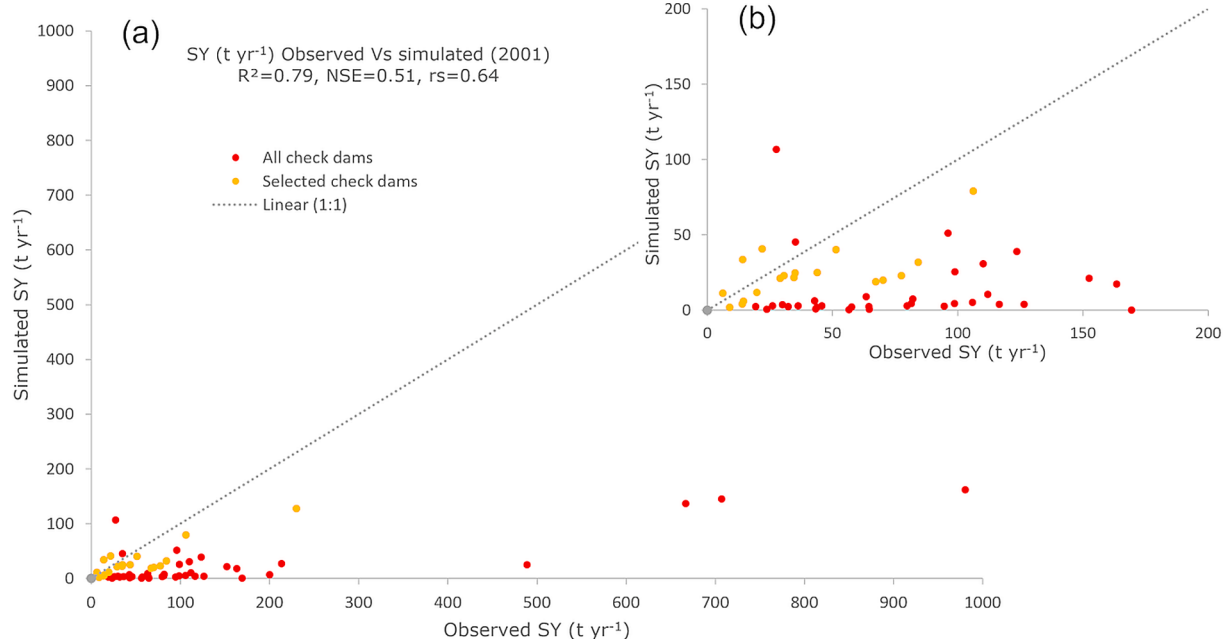


Fig. 4. Observed (2003) and simulated (2001) sediment yield at all (red dots & line) and selected (only yellow dots & line) check dam locations. (a) all observation and (b) zoom-in at smaller scale.

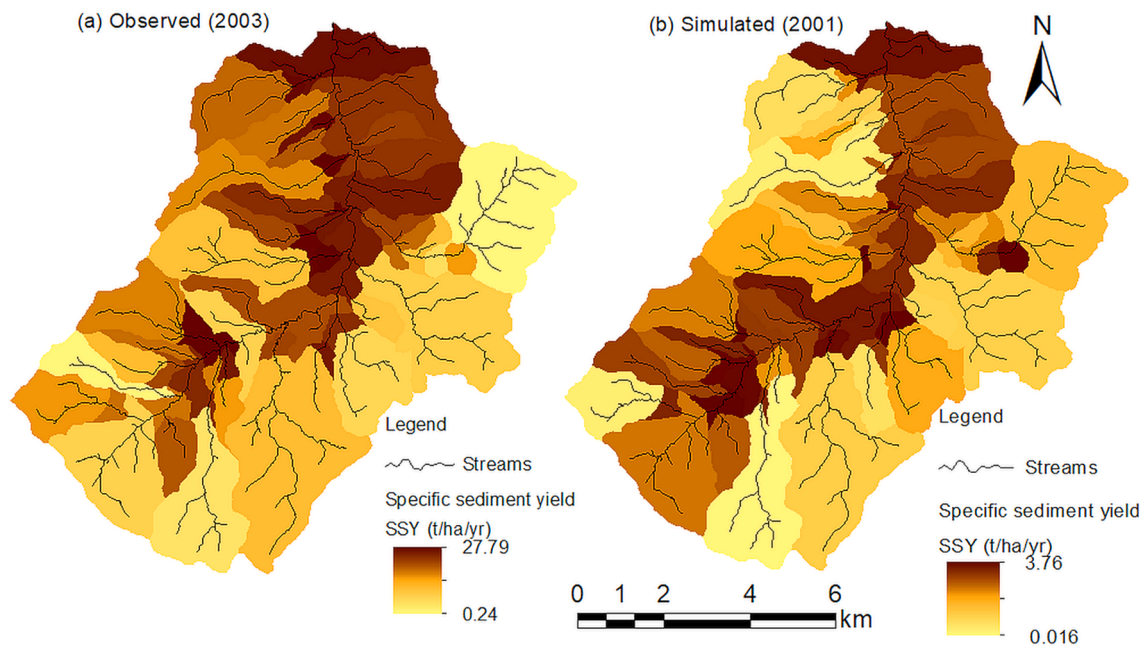


Fig. 5. Specific sediment yield maps of check dams contributing subcatchments with (a) observed and (b) simulated in the Rogativa catchment.

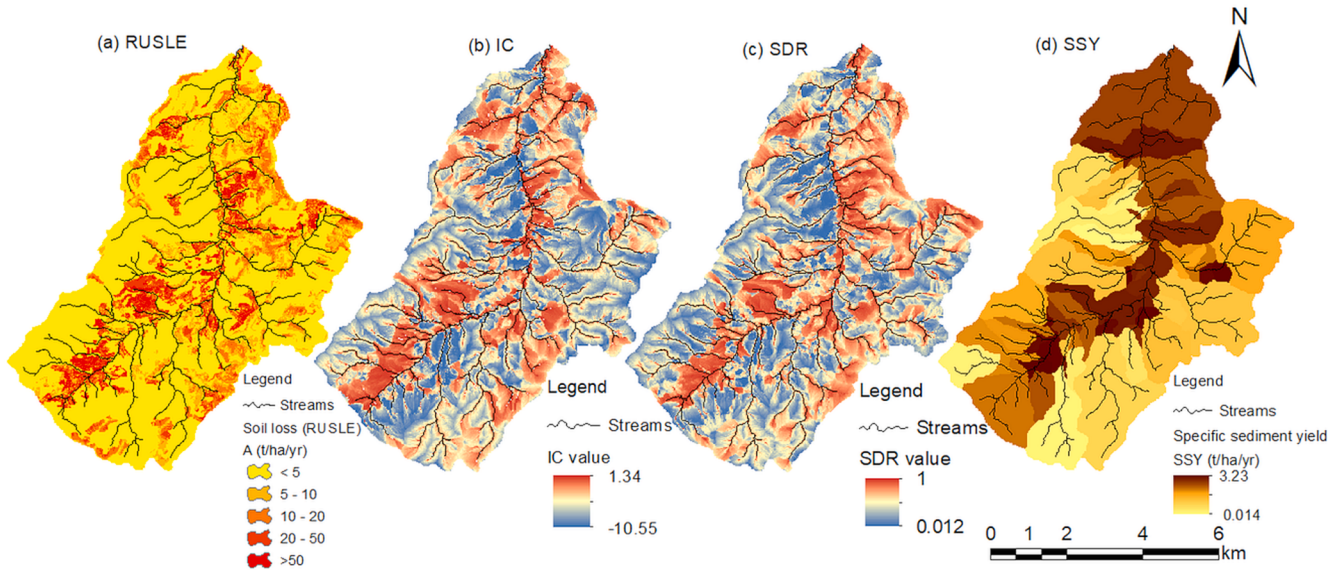


Fig. 6. Soil erosion and connectivity in 2001: RUSLE (a), IC (b), SDR (c), and SSY (d).

The final accumulated SYs estimated by the combined RUSLE-IC-SDR approach at the outlet of the Rogativa catchment were 2962.6, 423.3, 215.8, and 320.0 t yr⁻¹ in 1956, 1977, 2001, and 2016, respectively (Table 2). Land use changes and sediment retention by check dams affected the calculated SY and significantly reduced the SY going out of the Rogativa catchment.

Fig. 10 presents the specific sediment yield (SSY) for each subcatchment, i.e., SY per the upstream contributing area of each check dam and outlet. High SSYs are observed in the middle part of the basin and adjacent to the main stream of the whole reach (Fig. 10). The subcatchments averaged SSY ($t \text{ ha}^{-1} \text{ yr}^{-1}$) were estimated at 3.53, 0.46, 0.26, and 0.32 in 1956, 1977, 2001, and 2016, respectively. Fig. 10 shows a decrease in SSY from 1956 to 1977, and 2001, whereas there was a slight increase from 2001 to 2016. The variations in the spatio-temporal patterns show that in 1956, the lower catchments close to the mainstream contributed more to SSY, while in 1977 and 2001, the

contribution from the downstream part decreased whereas upstream subcatchments contributed more sediment. In 2016, the contribution from most upstream catchments slightly decreases while there was again some increase in lower subcatchments.

In summary (Table 2), the soil erosion rates, IC, SDR, and (S) SY maps show higher values in the croplands compared to other land uses, and near the channels compared to the hillslopes. Moreover, the model simulations show a decreasing trend due to the reforestation of the hillslopes, abandonment of agricultural activities, and construction of check dams since 1977. The temporal variation over the four time periods is due to changes in land use (C-factor), rainfall (R-factor), and K factors (through changes in organic carbon content) for the RUSLE results and C-factor as a weighting factor for the IC and SDR.

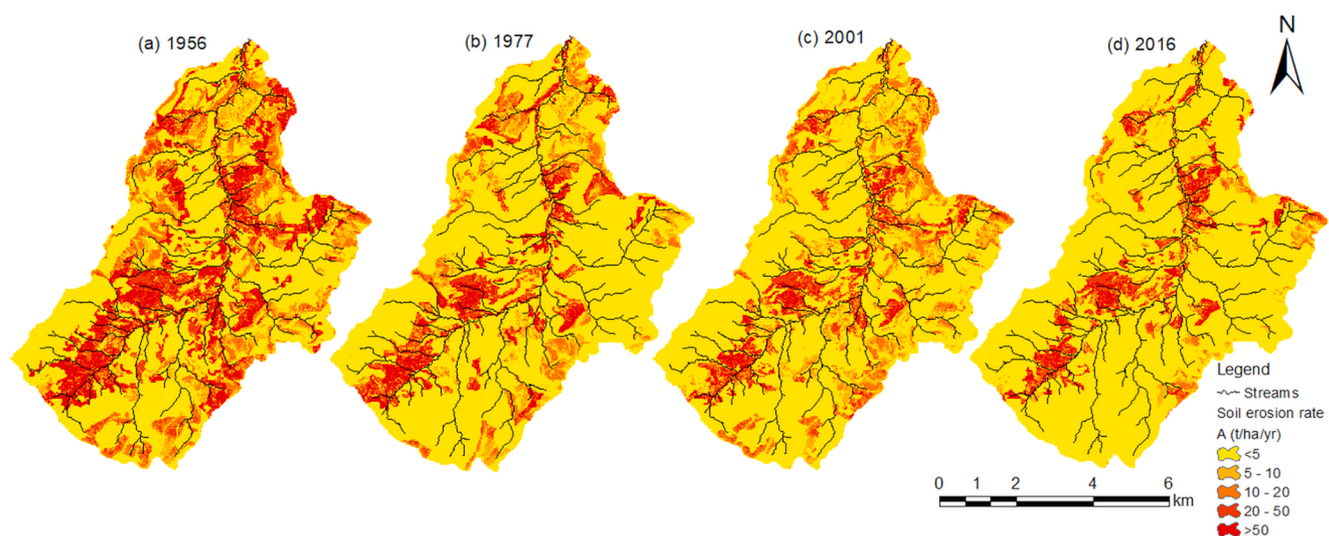


Fig. 7. Soil erosion rates as calculated by RUSLE for the Rogativa catchment in the four years (1956, 1977, 2001, and 2016).

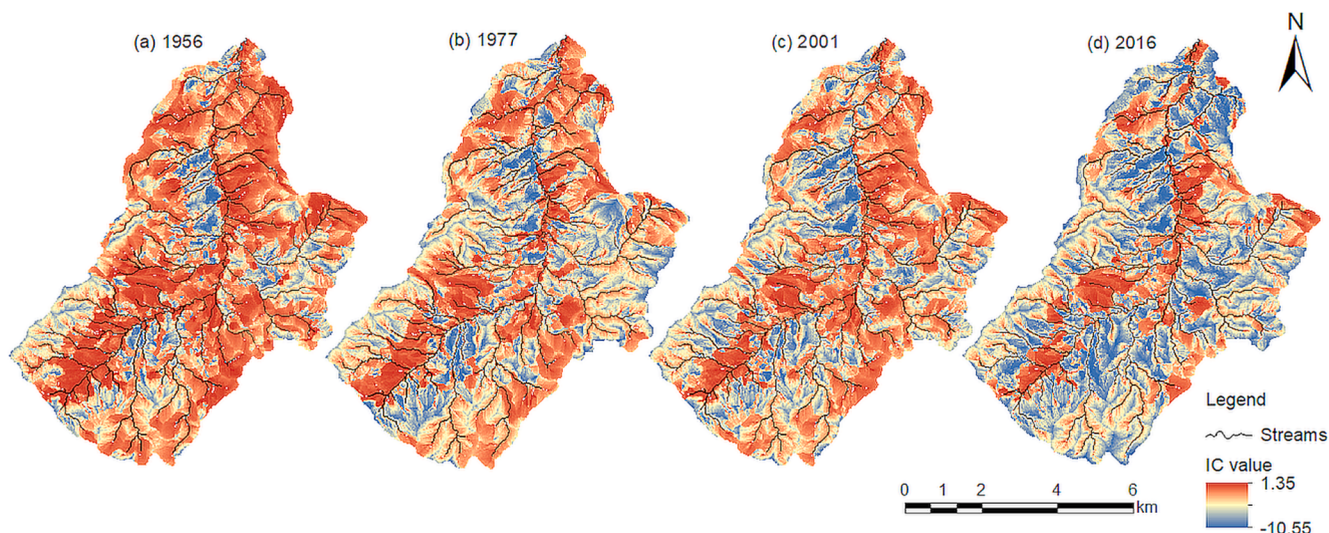


Fig. 8. Structural sediment connectivity expressed in terms of IC maps for the Rogativa catchment.

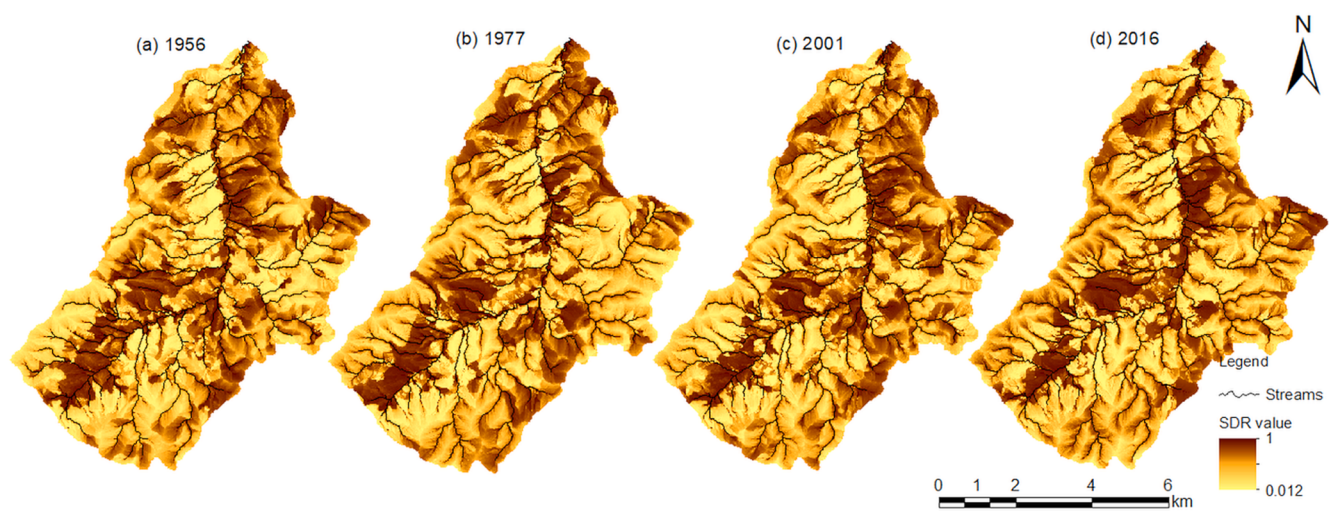


Fig. 9. Sediment delivery ratio maps for the Rogativa catchment (SDR_{max} on hillslope = 0.56, in streams = 1 & TE).

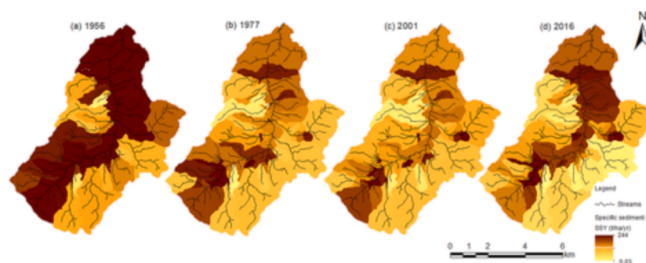


Fig. 10. Specific sediment yield for each check dam and outlet contributing area for the Rogatava catchment for the years 1956, 1977, 2001, and 2016.

3.3. Linking sediment connectivity and soil erosion spatiotemporal patterns

Fig. 11 shows the combination of RUSLE erosion estimates and IC maps and is classified into four quadrants: high erosion-high connectivity (HE-HC), high erosion-low connectivity (HE-LC), low erosion-high connectivity (LE-HC), low erosion-low connectivity (LE-LC). The area covered by each of the four quadrants was calculated for each year (**Table 3**). The 10th percentiles of ICs were -6.98 , -7.30 , -7.26 , and -7.69 in 1956, 1977, 2001, and 2016, respectively. The 90th percentiles were -3.00 , -3.65 , -3.79 , and -3.91 in 1956, 1977, 2001, and 2016, respectively. Both the 10th and 90th quantiles show decreasing connectivity over time.

Risk-prone areas, which have both high erosion risk and are highly connected, i.e., HE-HC, are shown in red in **Fig. 11**. These hotspot areas cover 8.08, 7.45, 7.25, and 6.83 percent (%) in 1956, 1977, 2001, and 2016, respectively. The HE-HC results show a slightly decreasing trend, and they are found adjacent to the channels, and the HE-LC pattern increases over time due to the high erosion areas (i.e., cropland) close to

the channels (**Fig. 11**). The hotspots have clustered in 2016 compared to a more scattered pattern in 1956.

Low impact locations are indicated by low erosion and low IC (LE-LC) and cover 13.33, 14.39, 14.90, and 18.23 % in 1956, 1977, 2001, and 2016, respectively. Most of the Rogatava watershed (77 %) is indicated in the medium pattern and the LE-HC quadrant has the lowest area coverage.

4. Discussion

4.1. Potential and challenges of the 'RUSLE-IC-SDR' approach

The combined 'RUSLE-IC-SDR' approach is a potentially informative option to evaluate spatiotemporal changes in erosion and (S)SY and identify source areas within a catchment (Michalek et al., 2021; Rajbanshi & Bhattacharya, 2020; Zhao et al., 2020). The 'RUSLE-IC-SDR' approach is a relatively low data-demanding method. It is simple to use, and it enables to identify hillslope source areas for soil erosion and sediment flux to support control and management practices (Michalek et al., 2021; Rajbanshi & Bhattacharya, 2020; Woznicki et al., 2020; Zhao et al., 2020). The coupled results of highly erodible and highly

Table 3
Area coverage proportion of different erosion-connectivity patterns.

Severity	Area coverage in ha (%)			
	1956	1977	2001	2016
HE-HC	423.4 (8.08)	390.4 (7.45)	380.0 (7.25)	358.1 (6.83)
HE-LC	46.4 (0.89)	56.9 (1.09)	71.3 (1.36)	95.6 (1.82)
LE-HC	9.3 (0.18)	1.2 (0.02)	1.5 (0.03)	0.1 (0.001)
LE-LC	698.9 (13.33)	754.5 (14.39)	781.2 (14.90)	955.7 (18.23)
Medium	4063.6 (77.53)	4038.6 (77.05)	4007.6 (76.46)	3832.2 (73.11)

Table 2
Summary of soil erosion rate and connectivity values (minimum/maximum, standard deviation, and average).

Year	Soil loss (RUSLE, $t \text{ ha}^{-1} \text{ yr}^{-1}$)	IC		SDR (max = 1)		SY ($t \text{ yr}^{-1}$)	SSY ($t \text{ ha}^{-1} \text{ yr}^{-1}$)
		Average ($\pm \text{Stdv}$)	Min to Max	Average	Min		
1956	20.3 (36.4)		-10.4 to 1.26	-5.14	0.10	0.26	2962.6 (70.0)
1977	10.2 (23.5)		-10.1 to 1.35	-5.75	0.012	0.243	423.3 (6.6)
2001	8.3 (17.1)		-10.41 to 1.23	-5.70	0.014	0.244	215.8 (3.6)
2016	6.7 (17.6)		-10.55 to 1.20	-6.22	0.098	0.227	320.0 (5.6)

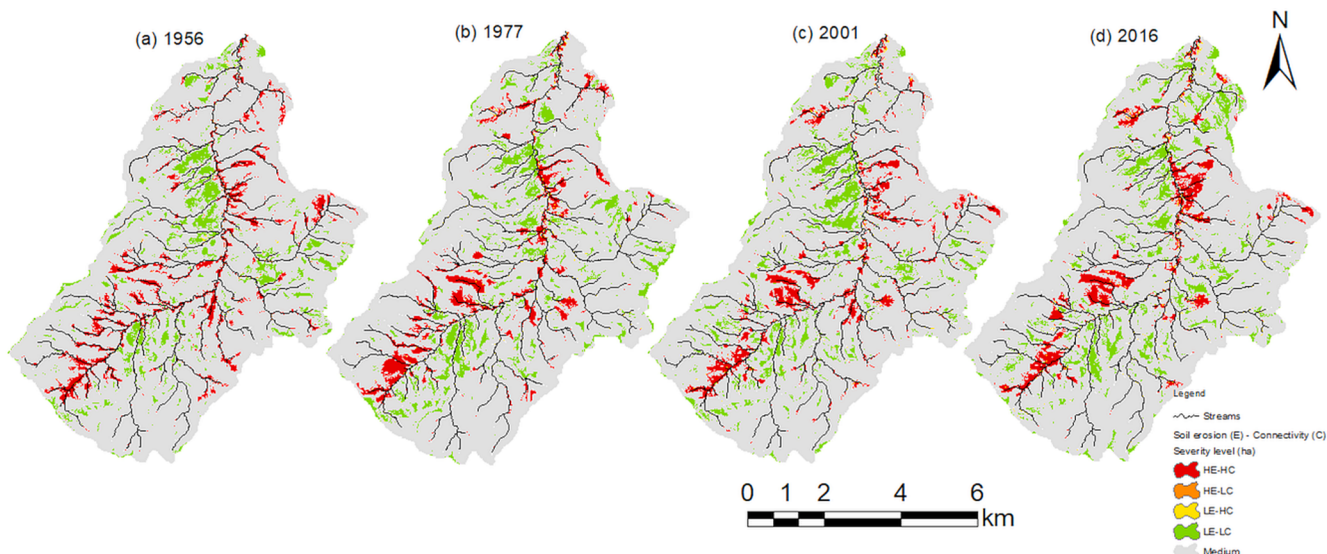


Fig. 11. Area coverage of different erosion-connectivity quadrants.

connected patterns (Fig. 11) were found to coincide with high SSY regions (Fig. 10). Separately the RUSLE or IC results do not show either highly erodible or highly connected areas contributing to more sediment yield, respectively. The combined effect of erosion-connectivity mapping provides information on (de)coupling of sediment flux (Hao et al., 2022; Michalek et al., 2021).

The hillslope SDR was derived from the IC which only considers structural connectivity. Besides, to consider part of the functional connectivity, we assumed the SDR to be 1 in the streams, and we used the sediment passing fraction (1-trapping efficiency) for the check dams within the channels. The combined SDR addresses the lack of sediment routing of RUSLE to generate SY (Michalek et al., 2021). IC and SDR indicated the most anthropogenically exposed subcatchments due to the high C-factor, and high values near the streams due to the landscape configuration of upslope contribution area to local reach. This result is consistent with earlier findings (Bollati and Cavalli, 2021; Cantreul et al., 2018; Michalek et al., 2021; Mishra et al., 2019; Woznicki et al., 2020).

Woznicki et al. (2020) confirmed that RUSLE and SDR input parameters are sources of uncertainty in estimating SY. The RUSLE model could be improved using high-resolution datasets and validated with field assessment (Michalek et al., 2021; Mishra et al., 2019; Rajbanshi and Bhattacharya, 2020; Woznicki et al., 2020). The IC and SDR parameters calibrated and validated with directly measured sediment yield data could increase the accuracy of the estimated SY (Michalek et al., 2021; Zhao et al., 2020). In addition, alternative forms of the relationship between IC and SDR could be explored. The IC, as an index of structural connectivity, does not consider climate impacts on connectivity. Other indices, some based on the IC, such as the Aggregated Index of Connectivity (AIC), include climate change impact (Bombino et al., 2020; López-Vicente & Ben-Salem, 2019; Wu et al., 2023; Zanandrea et al., 2021) and it would be interesting to test such index in future.

The RUSLE factors of Rogativa catchment such as R factor ($\text{MJ mm ha}^{-1} \text{y}^{-1}$), K factor ($\text{t h MJ}^{-1} \text{mm}^{-1}$), and LS factor (-) ranged in this study between 709 and 2095, 0.029–0.0314 and 0.01–66.58, respectively, which agrees with other studies findings in the Mediterranean region (Table 4).

In this study, the parameters IC_0 and k_b were used to calibrate the RUSLE-IC-SDR method by comparing predicted with measured SY behind check dams. Calibration results were relatively good when taking the most upstream and relatively non-silted check dams into account (Fig. 4). The individual model components (e.g., IC, SDR, RUSLE) affect model prediction due to error propagation and uncertainties; each model should be evaluated and verified to augment result accuracy (Batista et al.; 2019). Alongside these uncertainties and limitations, the 'RUSLE-IC-SDR' approach describes the local features of the Rogativa catchment.

The RUSLE does not account for gully and channel erosion and deposition and IC only considers structural connectivity. However, the results of the IC application indicate a decrease of connectivity of 17 % in the Rogativa catchment between 1956 and 2016 similar to the results

of Quiñonero-Rubio, Boix-Fayos & de Vente (2013) who developed a connectivity index including also geomorphological parameters and found a decrease of connectivity on average of $13 \pm 7\%$ in the same area between 1956 and 2006.

It would be interesting to further develop this approach by e.g., addressing rainfall-runoff events and RUSLE validation by field assessment to understand the functional connectivity of the catchment (López-Vicente & Ben-Salem, 2019; Michalek et al., 2021; Najafi et al., 2021b; Woznicki et al., 2020; Zanandrea et al., 2021). In addition, including a module that addresses channel sediment dynamics would address the current shortcomings. For example, the potential fluxes of sediment supply and delivery along the drainage network could be analysed with graph theory and empirical sediment transport of the CASCADE modelling framework (Schmitt et al., 2016; Tangi et al., 2019).

In summary, the 'RUSLE-IC-SDR' approach applied in this study has proven potential for use in assessing the impact of climate and landscape characteristics on hillslope erosion and SY, and it is useful to support management decisions regarding the identification of major hillslope source areas of sediment within a catchment. This notwithstanding, the approach can be prone to uncertainty due to a lack of direct measurements for validation, such as sediment load, and because RUSLE does not consider gully and channel erosion (and deposition) processes.

4.2. Spatiotemporal variations of sediment yield in the Rogativa catchment

The Rogativa catchment is characterized by important land use changes in the last decades, similar to those of the middle Mediterranean mountains (greening up of the slopes and construction of grey infrastructures, Boix-Fayos et al. (2020) and Eekhout et al. (2020)) which impact on the morphological channel dynamics and redistribution of sediments and associated nutrients (Boix-Fayos et al., 2015, 2009; Nadeu et al., 2014; Quiñonero-Rubio et al., 2016). Previous studies assessed the impacts of land use change and check dam construction on erosion and sedimentation processes in the Rogativa catchment (Boix-Fayos et al., 2007; Boix-Fayos et al., 2008; Eekhout et al., 2020; Halifa-Marín et al., 2019; Nadeu et al., 2014, 2015; Quiñonero-Rubio et al., 2016). These previous studies in the same catchment allow for a direct comparison between our findings and those using slightly different methods.

Considering all the check dams for calibration of the sediment yield is difficult as the period until when the check dams were functional, and the time that they were silted up, is unknown. Thus, the SY for silted-up check dams is less reliable than that for non-silted check dams. In general, it must be taken into account that the calibration was performed with the check dams located in the less erodible areas where the check dams were not silted because they offered a reliable time frame.

Boix-Fayos et al. (2008) applied the WaTEM-SEDEM model to the Rogativa catchment to estimate SY under different land use scenarios. They found SY values of 1123, 19, and 137 t yr^{-1} in 1956, 1981, and 1997, respectively at the catchment outlet. For the same catchment, the

Table 4
RUSLE factors (R, K, and LS) in the Mediterranean region.

Study area	R factor ($\text{MJ mm ha}^{-1} \text{y}^{-1}$)	K factor ($\text{t h MJ}^{-1} \text{mm}^{-1}$)	LS factor	Reference
Kassandra Peninsula, Northern Greece	490 to 538	0.0008 to 0.05	0.03–60.5	Stefanidis et al. (2021)
Central Palestinian highlands	230–440	0.012–0.032	0–34.3	Abu Hammad (2011)
Basilicata, SE Italy	200–1400	0.01–0.05	0–5282	Samela et al. (2022)
Inachos watershed, Greece	725.03–1111.51	0.0074–0.0145	0–146.49	Tetford et al. (2018)
Kuseyr Plateau, Turkey	309.73–674.52	0.001–0.065	–	Özşahin & Uygur (2014)
Arnás, Spanish Pyrenees	783–2740	0.002–0.024	0–612	López-Vicente et al. (2011)
Kolymvari, Greece	–	0.15–0.7	0–208	Karydas et al. (2009)
Alentejo, Portugal	433.6–854	0.0026–0.048	0–12.35	Ferreira & Panagopoulos (2014)
Estará, Spanish pre-Pyrenees	215–1969.2	0.0025–0.04	0–61.3	López-Vicente & Navas (2009)
Chianti, Italy	900–1800	0.025–0.046	–	Napoli et al. (2016)
Rafina, Attika, Greece	1126.1–1260.7	0.003–0.026	0.03–47.58	Efthimiou et al. (2020)
Calabria, Southern Italy	0–6000	0.0058–0.089	0(>30)	Terranova et al. (2009)

'RUSLE-IC-SDR' approach estimated SY at 2963, 423, 216, and 320 t yr⁻¹ in 1956, 1977, 2001, and 2016, respectively (Table 2). Interestingly, while the absolute values of predicted SY show differences, both approaches show the same relative influence of land use change and check dams on SY. Quiñonero-Rubio et al. (2016) applied WaTEM-SEDEM to the Taibilla catchment (of which the Rogativa is a sub-catchment) and found an underestimation of predicted SYs. In both studies, this could be due to channel erosion processes that play a vital role in contributing to SY which are not included in the RUSLE equation.

For the period 1956–2016, the Rogativa catchment is characterized by land abandonment and reforestation (Fig. 2), causing erosion to decrease on the hillslopes but increase in the channels over the years (Boix-Fayos et al., 2007; Boix-Fayos et al., 2008). Initially, the check dams were barriers (Fryirs, 2013) to decrease sediment connectivity, but later, their effect was reduced because they were being silted up with sediments (Boix-Fayos et al., 2008; Nadeu et al., 2012; Quiñonero-Rubio et al., 2016). Moreover, they may also become an important source of sediments when destroyed during extreme rain events.

The reforestation reduced sediment inputs from hillslopes into the channels (Boix-Fayos et al., 2008). Even though reforestation also caused a reduction in discharge, the reduced sediment input to streams from hillslopes leads to channel incision and increased bank erosion processes (Boix-Fayos et al., 2020, 2007; Nadeu et al., 2014). In the last decades, the ongoing siltation of the check dams and the expansion of cropland closer to the streams caused slight erosion increment. The combination of a decrease of hillslope erosion by reforestation and check dam construction however caused a 'hungry water' effect (Kondolf, 1977), evidenced by erosion downstream of the check dams. Bank and channel erosion could be seen in the main Rogativa channel, but also in subsidiary streams (Nadeu et al., 2012). The reducing sediment input from hillslopes into streams fits with the results obtained in the application of the current approach: despite the general reduction of the connectivity in the whole watershed, there is a middle area close to the main channel in the Rogativa catchment, where values of RUSLE and SY decrease 67 %, and 89 %, respectively, from 1956 to 2016 (Table 2). This can be also seen in the combination of erosion and connectivity classes in Fig. 11d, where areas of HE-HC can be seen around the main channel of the middle catchment in 2016.

Similar to the findings with the WaTEM-SEDEM model by Boix-Fayos et al. (2008) and Quiñonero-Rubio et al. (2016) the predicted SY from the 'RUSLE-IC-SDR' shows underestimation because of the lack of gully and channel erosion processes in the model (Liu and Fu, 2016; Michalek et al., 2021; Zhao et al., 2020). Many other studies also show that gully and channel erosion constitute a crucial part of total sediment yield in other Mediterranean catchments (de Vente et al., 2013; de Vente et al., 2008; Peñuela et al., 2023). Arguably, soil erosion and sediment connectivity (IC, SDR, and (S)SY) results and hotspot locations show higher values near the streams, which could be indicative of an occurrence of bank erosion but are not further quantified in the model. These sediment dynamics fit within the conceptual model of fluvial dynamics suggested by (Boix-Fayos et al., 2007) for the same catchment, considering the history of anthropic pressures in the area.

Thus, the RUSLE-IC-SDR method is capable of simulating soil erosion processes and connectivity on the hillslopes, but a channel component is missing. This is particularly important for future developments in modelling approaches in such catchments that have been affected by reforestation and hydrological control works. The changes carried out in the catchment areas leading to a greening-up of the surfaces tend to control sediment sources on the slopes and induce sources in the channels and in the connecting slope-channel areas (Boix-Fayos et al., 2007; Nadeu et al., 2012), thus introducing a channel erosion module in the catchment could help to better represent the fluvial morphological dynamics.

5. Conclusion

The 'RUSLE-IC-SDR' approach applied to the Mediterranean Rogativa catchment has the potential for assessing the impacts of climate and land use changes, and check dam construction on hillslope erosion and sediment connectivity over time. The RUSLE-IC-SDR method offers a simple, low-data-demanding approach to estimate sediment yield (SY). It is also suitable to show significant local spatiotemporal variation over time. Since RUSLE does not include sediment transport and deposition, IC-derived SDR was employed to incorporate routing in the channels.

The RUSLE soil erosion rates and sediment connectivity signature (IC, SDR, and (S)SY) maps show higher values in the croplands than in other land uses, and higher values close to streams than on the hillslopes, with a slightly decreasing trend over time. The sediment yield variations are influenced by land use (C-factor), climate, check dams, and topographic factors. A decreasing trend in soil erosion and sediment connectivity was observed over the years due to the reforestation of the hillslopes, abandonment of agricultural activities, and construction of check dams. Moreover, the relationship of erosion-connectivity patterns shows hotspot locations of both highly erodible and highly connected areas, some of them close to the streams.

The RUSLE-IC-SDR method is capable of simulating soil erosion processes and connectivity on the hillslopes, however, channel and gully erosion processes are not directly accounted for, while they may be dominant over hillslope processes considering their impact on the total sediment budget in the studied catchment. Further study is required, and it is suggested to couple the channel erosion processes. Direct sediment load measurements are needed for validation to improve model performance. Moreover, continuous C-factor values obtained from Normalized Difference Vegetation Index (NDVI) remote sensing imagery and the impact of watershed management support practice parameterized in the P-factor could further enhance model performance.

Declaration of Competing Interest

The authors declare that they have no known competing financial interests or personal relationships that could have appeared to influence the work reported in this paper.

Data availability

The data that has been used is confidential.

Acknowledgments

The first author (Niguse Abebe) was funded by a Wageningen Graduate School fellowship (Project no. 5160958163) and Joris Eekhout was supported by a Juan de la Cierva - Incorporación fellowship (IJC2020-044636-I). We also acknowledge funding from the Spanish Ministry of Science and Innovation (AEI) for the XTREME project (PID2019-109381RB-I00/AEI/10.13039/501100011033) and for the AGROALNEXT project with funding from European Union NextGenerationEU (PRTR-C17.I1) and Fundación Séneca (Region of Murcia). Last but not least, we also extend our sincere gratitude to Markus Egli and Juan F. Martínez-Murillo for their invaluable insights, as well as to the two anonymous reviewers whose thoughtful comments and suggestions significantly enhanced the quality of this manuscript.

References

- Abu Hammad, A., 2011. Watershed erosion risk assessment and management utilizing revised universal soil loss equation-geographic information systems in the Mediterranean environments. Water and Environment Journal 25, 149–162. <https://doi.org/10.1111/j.1747-6593.2009.00202.x>.
- Alfàs, L.J., 1991. Proyecto LUCDEME. Mapa de Suelos E = 1:100.000 (hoja Caravaca-910). Ministerio de Agricultura, Pesca y Alimentación, ICONA. Universidad de Murcia, Murcia, Spain.

- Arnoldus, H.M.J., 1977. Methodology used to determine the maximum potential range average annual soil loss to sheet and rill erosion in Morocco. FAO Soils Bulletin 34, 39–48.
- Batista, P.V.G., Davies, J., Silva, M.L.N., Quinton, J.N., 2019. On the evaluation of soil erosion models: Are we doing enough? *Earth Sci Rev* 197, 102898. <https://doi.org/10.1016/j.earscirev.2019.102898>.
- Boix-Fayos, C., Barberá, G.G., López-Bermúdez, F., Castillo, V.M., 2007. Effects of check dams, reforestation and land-use changes on river channel morphology: Case study of the Rogativa catchment (Murcia, Spain). *Geomorphology* 91, 103–123. <https://doi.org/10.1016/j.geomorph.2007.02.003>.
- Boix-Fayos, C., Vente, J.D., Barber, G.G., 2008. The impact of land use change and check-dams on catchment sediment yield. *Hydrol Process* 4935, 4922–4935. <https://doi.org/10.1002/hyp>.
- Boix-Fayos, C., de Vente, J., Albaladejo, J., Martínez-Mena, M., 2009. Soil carbon erosion and stock as affected by land use changes at the catchment scale in Mediterranean ecosystems. *Agric Ecosyst Environ* 133, 75–85. <https://doi.org/10.1016/j.agee.2009.05.013>.
- Boix-Fayos, C., Nadeu, E., Quiñonero, J.M., Martínez-Mena, M., Almagro, M., de Vente, J., 2015. Sediment flow paths and associated organic carbon dynamics across a Mediterranean catchment. *Hydrol Earth Syst Sci* 19, 1209–1223. <https://doi.org/10.5194/hess-19-1209-2015>.
- Boix-Fayos, C., Boerboom, L.G.J., Janssen, R., Martínez-Mena, M., Almagro, M., Pérez-Cutillas, P., Eekhout, J.P.C., Castillo, V., de Vente, J., 2020. Mountain ecosystem services affected by land use changes and hydrological control works in Mediterranean catchments. *Ecosyst. Serv.* 44, 1–14. <https://doi.org/10.1016/j.ecoser.2020.101136>.
- Bollati, I.M., Cavalli, M., 2021. Unraveling the relationship between geomorphodiversity and sediment connectivity in a small alpine catchment. *Transactions in GIS* 00, 1–20. <https://doi.org/10.1111/tgis.12793>.
- Bombino, G., Boix-Fayos, C., Cataldo, M.F., D'Agostino, D., Denisi, P., de Vente, J., Labate, A., Zema, D.A., 2020. A modified Catchment Connectivity Index for applications in semi-arid torrents of the Mediterranean environment. *River Res. Appl.* 36, 735–748. <https://doi.org/10.1002/rra.3606>.
- Borselli, L., Cassi, P., Torri, D., 2008. Prolegomeno to sediment and flow connectivity in the landscape: A GIS and field numerical assessment. *Catena (Amst)* 75, 268–277. <https://doi.org/10.1016/j.catena.2008.07.006>.
- Bracken, L.J., Wainwright, J., Ali, G.A., Tetzlaff, D., Smith, M.W., Reaney, S.M., Roy, A.G., 2013. Concepts of hydrological connectivity: Research approaches, pathways and future agendas. *Earth Sci. Rev.* 119, 17–34. <https://doi.org/10.1016/j.earscirev.2013.02.001>.
- Bracken, L.J., Turnbull, L., Wainwright, J., Bogaart, P., 2015. Sediment connectivity: A framework for understanding sediment transfer at multiple scales. *Earth Surf. Process Landf.* 40, 177–188. <https://doi.org/10.1002/esp.3635>.
- Brown, C., 1943. Discussion of sedimentation in reservoirs, by J. Witzig. *Proc. Am. Soc. Eng.* 69, 193–1500.
- Calsamiglia, A., Fortesa, J., García-Comendador, J., Lucas-Borja, M.E., Calvo-Cases, A., Estrany, J., 2018. Spatial patterns of sediment connectivity in terraced lands: Anthropogenic controls of catchment sensitivity. *Land Degrad. Dev.* 29, 1198–1210. <https://doi.org/10.1002/lrd.2840>.
- Cantreul, V., Bielders, C., Calsamiglia, A., Degré, A., 2018. How pixel size affects a sediment connectivity index in central Belgium. *Earth Surf. Process Landf.* 43, 884–893. <https://doi.org/10.1002/esp.4295>.
- Costigan, K.H., Kennard, M.J., Leigh, C., Sauquet, E., Datry, T., Boulton, A.J., 2017. Flow regimes in intermittent rivers and ephemeral streams. In: U.S. Geological Survey Scientific Investigations Report 2005–519, Intermittent Rivers and Ephemeral Streams: Ecology and Management. <https://doi.org/10.1016/B978-0-12-803835-2.00003-6>.
- Crema, S., Cavalli, M., 2018. SedInConnect: a stand-alone, free and open source tool for the assessment of sediment connectivity. *Comput. Geosci.* 111, 39–45. <https://doi.org/10.1016/j.cageo.2017.10.009>.
- Cucchiaro, S., Cazorzi, F., Marchi, L., Crema, S., Beinat, A., Cavalli, M., 2019. Multi-temporal analysis of the role of check dams in a debris-flow channel: Linking structural and functional connectivity. *Geomorphology* 345, 1–13. <https://doi.org/10.1016/j.geomorph.2019.106844>.
- de Vente, J., Poesen, J., Verstraeten, G., Van Rompaey, A., Govers, G., 2008. Spatially distributed modelling of soil erosion and sediment yield at regional scales in Spain. *Glob. Planet Change* 60, 393–415. <https://doi.org/10.1016/j.gloplacha.2007.05.002>.
- de Vente, J., Poesen, J., Govers, G., Boix-Fayos, C., 2009. The implications of data selection for regional erosion and sediment yield modelling. *Earth Surf. Process Landf.* 34, 1994–2007. <https://doi.org/10.1002/esp.1884>.
- de Vente, J., Poesen, J., Verstraeten, G., Govers, G., Vanmaercke, M., Van Rompaey, A., Arabkhedri, M., Boix-Fayos, C., 2013. Predicting soil erosion and sediment yield at regional scales: Where do we stand? *Earth Sci. Rev.* 127, 16–29. <https://doi.org/10.1016/j.earscirev.2013.08.014>.
- Eekhout, J.P.C., Boix-fayos, C., Pérez-cutillas, P., Vente, J.D., 2020. The impact of reservoir construction and changes in land use and climate on ecosystem services in a large Mediterranean catchment. *J. Hydrol. (Amst)* 590, 1–16. <https://doi.org/10.1016/j.jhydrol.2020.125208>.
- Eekhout, J.P.C., de Vente, J., 2020. How soil erosion model conceptualization affects soil loss projections under climate change. *Prog. Phys. Geogr.* 44, 212–232. <https://doi.org/10.1177/0309133319871937>.
- Ethimiou, N., Psomiadis, E., Panagos, P., 2020. Fire severity and soil erosion susceptibility mapping using multi-temporal Earth Observation data: The case of Mati fatal wildfire in Eastern Attica, Greece. *Catena (Amst)* 187. <https://doi.org/10.1016/j.catena.2019.104320>.
- Ferreira, V., Panagopoulos, T., 2014. Seasonality of soil erosion under Mediterranean conditions at the Alqueva dam watershed. *Environ. Manage.* 54, 67–83. <https://doi.org/10.1007/s00267-014-0281-3>.
- Fryirs, K., 2013. (Dis)Connectivity in catchment sediment cascades: A fresh look at the sediment delivery problem. *Earth Surf. Process Landf.* 38, 30–46. <https://doi.org/10.1002/esp.3242>.
- Grauso, S., Pasanisi, F., Tebano, C., 2018. Assessment of a simplified connectivity index and specific sediment potential in river basins by means of geomorphometric tools. *Geosciences (Switzerland)* 8, 1–14. <https://doi.org/10.3390/geosciences8020048>.
- Hajigholizadeh, M., Melesse, A.M., Fuentes, H.R., 2018. Erosion and sediment transport modelling in shallowwaters: A review on approaches, models and applications. *Int. J. Environ. Res. Public Health.* <https://doi.org/10.3390/ijerph15030518>.
- Halifa-Marín, A., Pérez-Cutillas, P., Almagro, M., Martínez-Mena, M., Boix-Fayos, C., 2019. Fluvial geomorphological dynamics and land use changes: impact on the organic carbon stocks of soil and sediment. *Bosque* 40, 3–16. <https://doi.org/10.4067/S0717-92002019000100003>.
- Hamel, P., Chaplin-kramer, R., Sim, S., Mueller, C., 2015. A new approach to modeling the sediment retention service (InVEST 3.0): Case study of the Cape Fear catchment, North Carolina, USA. *Sci. Total Environ.* 524–525, 166–177. <https://doi.org/10.1016/j.scitotenv.2015.04.027>.
- Hamel, P., Falinski, K., Sharp, R., Auerbach, D.A., Sánchez-Canales, M., Dennedy-Frank, P.J., 2017. Sediment delivery modeling in practice: Comparing the effects of watershed characteristics and data resolution across hydroclimatic regions. *Sci. Total Environ.* 580, 1381–1388. <https://doi.org/10.1016/j.scitotenv.2016.12.103>.
- Hao, R., Huang, X., Cai, Z.W., Xiao, H.B., Wang, J., Shi, Z.H., 2022. Incorporating sediment connectivity index into MUSLE model to explore soil erosion and sediment yield relationships at event scale. *J. Hydrol. (Amst)* 614, 128579. <https://doi.org/10.1016/j.jhydrol.2022.128579>.
- Heckmann, T., Cavalli, M., Cerdan, O., Foerster, S., Javaux, M., Lode, E., Smetanová, A., Vericat, D., Brardinoni, F., 2018. Indices of sediment connectivity: opportunities, challenges and limitations. *Earth Sci. Rev.* 187, 77–108. <https://doi.org/10.1016/j.earscirev.2018.08.004>.
- Hengl, T., de Jesus, J.M., Heuvelink, G.B.M., Gonzalez, M.R., Kilibarda, M., Blagotić, A., Shangguan, W., Wright, M.N., Geng, X., Bauer-Marschallinger, B., Guevara, M.A., Vargas, R., MacMillan, R.A., Batjes, N.H., Leenaars, J.G.B., Ribeiro, E., Wheeler, I., Mantel, S., Kempen, B., 2017. SoilGrids250m: Global gridded soil information based on machine learning. *PLoS One* 12. <https://doi.org/10.1371/journal.pone.0169748>.
- Hooke, R.L.B., 2003. Predictive modeling in geomorphology: An oxymoron? *Geophys. Monogr. Series* 135, 51–61. <https://doi.org/10.1029/135GM05>.
- Hooke, J., Souza, J., 2021. Challenges of mapping, modelling and quantifying sediment connectivity. *Earth Sci. Rev.* 223, 103847. <https://doi.org/10.1016/j.earscirev.2021.103847>.
- Hooke, J., Souza, J., Marchamalo, M., 2021. Evaluation of connectivity indices applied to a Mediterranean agricultural catchment. *Catena (Amst)* 207, 105713. <https://doi.org/10.1016/j.catena.2021.105713>.
- IGME, 1978. Instituto Geológico y Minero de España / naGeológico y Minero de España (IGME). Mapa geológico de España 1: 50000, ~Nerpio 909: 23–26.
- Jaeger, K.L., Sutfin, N.A., Tooth, S., Michaelides, K., Singer, M., 2017. Geomorphology and sediment regimes of intermittent rivers and ephemeral streams. U.S. geological survey information technology report, 2002-0010, Intermittent Rivers and Ephemeral Streams: Ecology and Management. *Ecology and Management*. DOI: 10.1016/B978-0-12-803835-2.00002-4.
- Karsenberg, D., Schmitz, O., Salamon, P., de Jong, K., Bierkens, M.F.P., 2010. A software framework for construction of process-based stochastic spatio-temporal models and data assimilation. *Environ. Model. Softw.* 25, 489–502. <https://doi.org/10.1016/j.envsoft.2009.10.004>.
- Karydas, C.G., Sekuloska, T., Silleos, G.N., 2009. Quantification and site-specification of the support practice factor when mapping soil erosion risk associated with olive plantations in the Mediterranean island of Crete. *Environ. Monit. Assess.* 149, 19–28. <https://doi.org/10.1007/s10661-008-0179-8>.
- Keesstra, S., Nunes, J.P., Saco, P., Parsons, T., Poeppl, R., Masselink, R., Cerdà, A., 2018. The way forward: Can connectivity be useful to design better measuring and modelling schemes for water and sediment dynamics? *Sci. Total Environ.* 644, 1557–1572. <https://doi.org/10.1016/j.scitotenv.2018.06.342>.
- Kondolf, G.M., 1977. PROFILE: Hungry water: effects of dams and gravel mining on river channels. *Environ. Manage.* 21, 533–551. <https://doi.org/10.1007/s002679900048>.
- Levick, L.R., Goodrich, D.C., Hernandez, M., Fonseca, J., Semmens, D.J., Stromberg, J., Tluczek, M., Leidy, R. a., Sciani, M., Guertin, P.D., Kepner, W.G., 2008. The ecological and hydrological significance of ephemeral and intermittent streams in the arid and semi-arid American Southwest, US Environmental Protection Agency, Office of Research and Development.
- Liu, Y., Fu, B., 2016. Assessing sedimentological connectivity using WATEM/SEDEM model in a hilly and gully watershed of the Loess Plateau, China. *Ecol. Indic.* 66, 259–268. <https://doi.org/10.1016/j.ecolind.2016.01.055>.
- López-Vicente, M., Ben-Salem, N., 2019. Computing structural and functional flow and sediment connectivity with a new aggregated index: A case study in a large Mediterranean catchment. *Sci. Total Environ.* 651, 179–191. <https://doi.org/10.1016/j.scitotenv.2018.09.170>.
- López-Vicente, M., Lana-Reault, N., García-Ruiz, J.M., Navas, A., 2011. Assessing the potential effect of different land cover management practices on sediment yield from an abandoned farmland catchment in the Spanish Pyrenees. *J. Soils Sediments* 11, 1440–1455. <https://doi.org/10.1007/s11368-011-0428-2>.
- López-Vicente, M., Navas, A., 2009. Predicting soil erosion with RUSLE in mediterranean agricultural systems at catchment scale. *Soil Sci.* 174, 272–282. <https://doi.org/10.1097/SS.0b013e3181a4bf50>.

- Maner, S.B., 1958. Factors affecting sediment delivery rates in the red hills physiographic area. *Eos. Trans. Am. Geophys. Union* 39, 669–675. <https://doi.org/10.1029/TR039i004p00669>.
- Merritt, W.S., Letcher, R.A., Jakeman, A.J., 2003. A review of erosion and sediment transport models. In: *Environmental Modelling and Software*. Elsevier BV, pp. 761–799. [https://doi.org/10.1016/S1364-8152\(03\)00078-1](https://doi.org/10.1016/S1364-8152(03)00078-1).
- Michalek, A., Zarnaghsh, A., Husic, A., 2021. Modeling linkages between erosion and connectivity in an urbanizing landscape. *Sci. Total Environ.* 764, 144255. <https://doi.org/10.1016/j.scitotenv.2020.144255>.
- Ministerio de Fomento de España, 2015. Plan Nacional de Ortofotografía Aérea.
- Mishra, K., Sinha, R., Jain, V., Nepal, S., Uddin, K., 2019. Towards the assessment of sediment connectivity in a large Himalayan river basin. *Sci. Total Environ.* 661, 251–265. <https://doi.org/10.1016/j.scitotenv.2019.01.118>.
- Nadeu, E., Berhe, A.A., de Vente, J., Boix-Fayos, C., 2012. Erosion, deposition and replacement of soil organic carbon in Mediterranean catchments: A geomorphological, isotopic and land use change approach. *Biogeosciences* 9, 1099–1111. <https://doi.org/10.5194/bg-9-1099-2012>.
- Nadeu, E., Van Oost, K., Boix-Fayos, C., de Vente, J., 2014. Importance of land use patterns for erosion-induced carbon fluxes in a Mediterranean catchment. *Agric. Ecosyst. Environ.* 189, 181–189. <https://doi.org/10.1016/j.agee.2014.03.040>.
- Nadeu, E., Quiñonero-Rubio, J.M., de Vente, J., Boix-Fayos, C., 2015. The influence of catchment morphology, lithology and land use on soil organic carbon export in a Mediterranean mountain region. *Catena (Amst)* 126, 117–125. <https://doi.org/10.1016/j.catena.2014.11.006>.
- Najafi, S., Dragovich, D., Heckmann, T., Sadeghi, S.H., 2021a. Sediment connectivity concepts and approaches. *Catena (Amst)* 196, 104880. <https://doi.org/10.1016/j.catena.2020.104880>.
- Najafi, S., Sadeghi, S.H., Heckmann, T., 2021b. Analysis of sediment accessibility and availability concepts based on sediment connectivity throughout a watershed. *Land Degrad. Dev.* 1–22. <https://doi.org/10.1002/lrd.3964>.
- Napoli, M., Cecchi, S., Orlandini, S., Mugnai, G., Zanchi, C.A., 2016. Simulation of field-measured soil loss in Mediterranean hilly areas (Chianti, Italy) with RUSLE. *Catena (Amst)* 145, 246–256. <https://doi.org/10.1016/j.catena.2016.06.018>.
- Ouadja, A., Benfetta, H., Porto, P., Flanagan, D.C., Mihoubi, M.K., Omeir, M.R., Graia, M., Ghosal, K., Talchabhadel, R., 2021. Mapping potential soil erosion using RUSLE, Remote Sensing, and GIS: a case study in the watershed of Oued El Arjem. Northwest Algeria Arab. J. Geosci. 14, 1–21. <https://doi.org/10.1007/s12517-021-07992-6>.
- Ouadja, A., Benfetta, H., Porto, P., Mihoubi, M.K., Flanagan, D.C., Dehni, A., Talchabhadel, R., 2022. GIS and remote sensing integration for sediment performance assessment based on a RUSLE and sediment delivery ratio model in northwest Algeria. Arab. J. Geosci. 15, 1–21. <https://doi.org/10.1007/s12517-022-09502-8>.
- Özşahin, E., Uygur, V., 2014. The effects of land use and land cover changes (LULCC) in kuseyr plateau of Turkey on erosion. *Turkish J. Agricul. Fores.* 38, 478–487. <https://doi.org/10.3906/tar-1306-86>.
- Panagos, P., Borrelli, P., Meusburger, K., van der Zanden, E.H., Poesen, J., Alewell, C., 2015. Modelling the effect of support practices (P-factor) on the reduction of soil erosion by water at European scale. *Environ. Sci. Policy* 51, 23–34. <https://doi.org/10.1016/j.envsci.2015.03.012>.
- Pandey, A., Himanshu, S.K., Mishra, S.K., Singh, V.P., 2016. Physically based soil erosion and sediment yield models revisited. *Catena (Amst)* 147, 595–620. <https://doi.org/10.1016/j.catena.2016.08.002>.
- Parsons, A.J., Bracken, L., Poepll, R.E., Wainwright, J., Keesstra, S.D., 2015. Introduction to special issue on connectivity in water and sediment dynamics. *Earth Surf. Process Landf.* 40, 1275–1277. <https://doi.org/10.1002/esp.3714>.
- Penuela, A., Hayas, A., Infante-Amate, J., Ruiz-Montes, P., Temme, A., Reimann, T., Peña-Acevedo, A., Vanwalleghem, T., 2023. A multi-millennial reconstruction of gully erosion in two contrasting Mediterranean catchments. *Catena (Amst)* 220. <https://doi.org/10.1016/j.catena.2022.106709>.
- Peral García, C., Navascués Fernández-Victorio, B., Ramos Calzado, P., 2017. Serie de precipitación diaria en rejilla con fines climáticos. Serie de precipitación diaria en rejilla con fines climáticos, Agencia Estatal de Meteorología <https://doi.org/10.31978/014-17-009-5>.
- Persichillo, M.G., Bordoni, M., Cavalli, M., Crema, S., Meisina, C., 2018. The role of human activities on sediment connectivity of shallow landslides. *Catena (Amst)* 160, 261–274. <https://doi.org/10.1016/j.catena.2017.09.025>.
- Poeppl, R.E., Fryirs, K.A., Tunnicliffe, J., Brierley, G.J., 2020. Managing sediment (dis) connectivity in fluvial systems. *Sci. Total Environ.* 736, 139627. <https://doi.org/10.1016/j.scitotenv.2020.139627>.
- Quiñonero-Rubio, J.M., Boix-Fayos, C., de Vente, J., 2013. Desarrollo y aplicación de un índice multifactorial de conectividad de sedimentos a escala de cuenca. *Cuadernos de Investigación Geográfica* 39, 203–223.
- Quiñonero-Rubio, J.M., Nadeu, E., Boix-Fayos, C., de Vente, J., 2016. Evaluation of the effectiveness of forest restoration and check-dams to reduce catchment sediment yield. *Land Degrad. Dev.* 27, 1018–1031. <https://doi.org/10.1002/lrd.2331>.
- Rahmati, O., Arabkhedri, M., Soleimanpour, S.M., Kalantari, Z., Cavalli, M., Crema, S., Bahmani, A., 2022. Towards quantifying the efficiency of contour trenching in controlling water erosion: A novel application of the sediment connectivity concept. <https://ssrn.com/abstract=4120192> 1–22.
- Rainato, R., Picco, L., Cavalli, M., Mao, L., Neverman, A.J., Tarolli, P., 2018. Coupling climate conditions, sediment sources and sediment transport in an Alpine basin. *Land Degrad. Dev.* 29, 1154–1166. <https://doi.org/10.1002/lrd.2813>.
- Rajbanshi, J., Bhattacharya, S., 2020. Assessment of soil erosion, sediment yield and basin specific controlling factors using RUSLE-SDR and PLSR approach in Konar river basin, India. *J. Hydrol.* (Amst) 587. <https://doi.org/10.1016/j.jhydrol.2020.124935>.
- Rellini, I., Scopesi, C., Olivari, S., Firpo, M., Maerker, M., 2019. Assessment of soil erosion risk in a typical mediterranean environment using a high resolution RUSLE approach (Portofino promontory, NW-Italy). *J. Maps* 15, 356–362. <https://doi.org/10.1080/17445647.2019.1599452>.
- Renard, K.G., Freimund, J.R., 1994. Using monthly precipitation data to estimate the R-factor in the revised USLE. *J. Hydrol.* (Amst) 157, 287–306.
- Samella, C., Imbrinda, V., Coluzzi, R., Pace, L., Simonello, T., Lanfredi, M., 2022. Multi-decadal assessment of soil loss in a mediterranean region characterized by contrasting local climates. *Land (Basel)* 11. <https://doi.org/10.3390/land11071010>.
- Schmitt, R.J.P., Bizzzi, S., Castelletti, A., 2016. Tracking multiple sediment cascades at the river network scale identifies controls and emerging patterns of sediment connectivity. *Water Resour. Res.* 52, 3941–3965. <https://doi.org/10.1002/2015WR018097>.
- Stefanidis, S., Alexandridis, V., Chatzichristaki, C., Stefanidis, P., 2021. Assessing soil loss by water erosion in a typical mediterranean ecosystem of Northern Greece under current and future rainfall erosivity. *Water (Switzerland)* 13. <https://doi.org/10.3390/w13152002>.
- Tangi, M., Schmitt, R., Bizzzi, S., Castelletti, A., 2019. The CASCADE toolbox for analyzing river sediment connectivity and management. *Environ. Model. Software* 119, 400–406. <https://doi.org/10.1016/j.envsoft.2019.07.008>.
- Tarboton, D.G., Sazib, N., Dash, P., 2015. Quick start guide to using the TauDEM ArcGIS toolbox (TauDEM 5.3).
- Terranova, O., Antronico, L., Coscarelli, R., Iaquinta, P., 2009. Soil erosion risk scenarios in the Mediterranean environment using RUSLE and GIS: An application model for Calabria (southern Italy). *Geomorphology* 112, 228–245. <https://doi.org/10.1016/j.geomorph.2009.06.009>.
- Tetford, P.E., Desloges, J.R., Nakassis, D., 2018. The potential relationship between archaeological artifact exposure and surface geomorphic processes: Northeastern Peloponnese, Greece. *J. Field Archaeol.* 43, 538–550. <https://doi.org/10.1080/00934690.2018.1518947>.
- Thompson, J., Cassidy, R., Doody, D.G., Flynn, R., 2013. Predicting critical source areas of sediment in headwater catchments. *Agric. Ecosyst. Environ.* 179, 41–52. <https://doi.org/10.1016/j.agee.2013.07.010>.
- Turnbull, L., Wainwright, J., 2019. From structure to function: Understanding shrub encroachment in drylands using hydrological and sediment connectivity. *Ecol. Indic.* 98, 608–618. <https://doi.org/10.1016/j.ecolind.2018.11.039>.
- Verstraeten, G., Prosser, I.P., Fogarty, P., 2007. Predicting the spatial patterns of hillslope sediment delivery to river channels in the Murray-Bidgee catchment, Australia. *J. Hydrol.* (Amst) 334, 440–454. <https://doi.org/10.1016/j.jhydrol.2006.10.025>.
- Vigliac, O., Borselli, L., Newham, L.T.H., McInnes, J., Roberts, A.M., 2012. Geomorphology Comparison of conceptual landscape metrics to define hillslope-scale sediment delivery ratio. *Geomorphology* 138, 74–88. <https://doi.org/10.1016/j.geomorph.2011.08.026>.
- Wainwright, J., Parsons, A.J., Cooper, J.R., Gao, P., Gillies, J.A., Mao, L., Orford, J.D., Knight, P.G., 2015. The concept of transport capacity in geomorphology. *Reviews of Geophysics* 53, 1155–1202. <https://doi.org/10.1002/2014RG000474>.
- Walling, D.E., 1983. The sediment delivery problem. *J. Hydrol.* (Amst) 65, 209–237.
- Wohl, E., 2017. Connectivity in rivers. *Prog. Phys. Geogr.* 41, 345–362. <https://doi.org/10.1177/030913317714972>.
- Wohl, E., Brierley, G., Cadol, D., Coulthard, T.J., Covino, T., Fryirs, K.A., Grant, G., Hilton, R.G., Lane, S.N., Magilligan, F.J., Meitzen, K.M., Passalacqua, P., Poepll, R.E., Rathburn, S.L., Sklar, L.S., 2019. Connectivity as an emergent property of geomorphic systems. *Earth Surf. Process Landf.* 44, 4–26. <https://doi.org/10.1002/esp.4434>.
- Woznicki, S.A., Cada, P., Wickham, J., Schmidt, M., Baynes, J., Mehaffey, M., Neale, A., 2020. Sediment retention by natural landscapes in the conterminous United States. *Sci. Total Environ.* 745. <https://doi.org/10.1016/j.scitotenv.2020.140972>.
- Wu, Z., Baartman, J.E.M., Pedro Nunes, J., López-Vicente, M., 2023. Intra-annual sediment dynamic assessment in the Wei River Basin, China, using the AIC functional-structural connectivity index. *Ecol. Indic.* 146. <https://doi.org/10.1016/j.ecolind.2022.109775>.
- Wu, L., Liu, X., Ma, X., Yi, X., 2018. Research progress on the watershed sediment delivery ratio. *Int. J. Environ. Stud.* 75, 565–579. <https://doi.org/10.1080/00207233.2017.1392771>.
- Yang, K., Lu, C., 2018. Evaluation of land-use change effects on runoff and soil erosion of a hilly basin — the Yanhe River in the Chinese Loess Plateau. *Land Degrad. Dev.* 29, 1211–1221. <https://doi.org/10.1002/lrd.2873>.
- Zanandreia, F., Michel, G.P., Kobiyama, M., Censi, G., Abatti, B.H., 2021. Spatial-temporal assessment of water and sediment connectivity through a modified connectivity index in a subtropical mountainous catchment. *Catena* (Amst) 204, 105380. <https://doi.org/10.1016/j.catena.2021.105380>.
- Zhang, H., Wei, J., Yang, Q., Baartman, J.E.M., Gai, L., Yang, X., Li, S.Q., Yu, J., Ritsema, C.J., Geissen, V., 2017. An improved method for calculating slope length (λ) and the LS parameters of the Revised Universal Soil Loss Equation for large watersheds. *Geoderma* 308, 36–45. <https://doi.org/10.1016/j.geoderma.2017.08.006>.
- Zhao, G., Gao, P., Tian, P., Sun, W., Hu, J., Mu, X., 2020. Assessing sediment connectivity and soil erosion by water in a representative catchment on the Loess Plateau, China. *Catena* (Amst) 185, 104284. <https://doi.org/10.1016/j.catena.2019.104284>.